Jurnal Ilmu Fisika
Vol. 16, No. 1, March 2024, pp. 63–70
ISSN: 1979-4657 (Print); 2614-7386 (Online)
https://doi.org/10.25077/jif.16.1.63-70.2024

Jurnal Ilmu Fisika
Open Access

Analysis of Secondary Particles Produced by 50-500 MeV Muon and Water Interaction using PHITS Monte Carlo Package

Sitti Yani, Dadan Hidayatuloh, Tony Sumaryada

Department of Physics, Faculty of Mathematics and Natural Sciences, IPB University
Jalan Meranti Kampus IPB Dramaga, Bogor 16680, Indonesia

Article Info

Article History:

Received September 23, 2023
Revised December 26, 2023
Accepted December 27, 2023
Published online February 03, 2024

Keywords:

muon
muography
Monte Carlo
PHITS
neutron
photon

Corresponding Author:

Name of Corresponding Author,
Email: sittiyani@apps.ipb.ac.id

ABSTRACT

Secondary particles will always be generated in particle-to-matter interactions. The interaction of muons with matter produces various secondary particles. In this study, secondary particles produced by the interaction between muons with energies of 5, 50, 100, 200 and 500 MeV with water were analyzed using the PHITS Monte Carlo package. The muon source is placed on the surface of water that has a thickness of 1 km. The muography technique was applied by placed a detector at a depth of 1 km from the source. This detector records the secondary particles produced by the interaction. The results obtained show that this interaction produces secondary particles in the form of photons and neutrons in the detector. The number and energy of these photons and neutrons are strongly influenced by the initial energy of the muon. Muons with the lowest energy of 5 MeV produce more secondary particles than any other energy by a factor of 10. Low-energy muons travel slowly, allowing more interactions to occur and increasing the number of secondary particles in the detector. The energies of neutrons and photons in the detector are at most 3.76 MeV and 5.3 MeV, respectively.

1. INTRODUCTION

Muons are particles produced by the interaction between cosmic radiation and the atmosphere surrounding the Earth. Muons have different characteristics from other particles, such as electrons, photons, and neutrons (Zhang et al., 2020). Muons are subatomic particles with high energy and material penetration power. They have a mass almost 200 times greater than electrons and interact with atoms primarily through Coulomb scattering. When interacting with living things, they are harmless (Hansen & Thompson, 1976; Armour, 2010; Abe & Sato, 2017).

Currently, muons have been widely used in mapping or detecting the composition of unknown materials that are widely utilized in the fields of geology (Morishima et al., 2017), volcanology (Kusagaya & Tanaka, 2015; Oláh et al., 2018; Barnoud et al., 2021) and civil engineering (Hamar et al., 2022). The principle applied is similar to that used in X-rays in radiology (Kaiser, 2019). The muon imaging techniques used were muography and muon scattering tomography (MST). Muography uses only one detector placed after the object under review, while MST uses several detectors around the

object, which is helpful in obtaining more detailed information about the object. Muography is suitable for large objects, while the MST technique is not (Das et al., 2022).

Every charged and uncharged particle passing through a particular material will interact with specific mechanisms and processes. Coulomb scattering with the atom of material will occur when passing through a material, which can produce secondary particles as they lose energy due to interactions with the surrounding matter. Muon interactions with matter can be in ionization, bremsstrahlung process, pair production and nuclear interactions. The type of interaction that occurs depends on the energy of the incident muon and the density of the material it passes through (Morris et al., 2014; Mahon et al., 2019; Riggi, 2023).

There have been many studies on secondary particles generated from muon interactions (Galgóczi et al., 2020; Pérez Prada et al., 2022). The secondary particles produced in muon interaction experimentally have been studied by Galgóczi et al. (2020). The secondary particles produced are measured by plastic scintillators placed around the target. Prada et al. (2022) analyzed the kinematics of secondary particles and their dependency on material characteristics in the shipping container. They found that photons and neutrons produced during muon interaction were performed using the Geant4 code. Many muons transport studies have also been carried out by simulation using Monte Carlo-based software such as FLUKA (Danev et al., 2016; Infantino et al., 2016), Geant4 (Nishiyama et al., 2016; Vanini et al., 2019; Hu et al., 2023), and PHITS (Abe & Sato, 2017; Sakaki et al., 2020).

This research is focused on analyzing the flux and spectrum of secondary particles produced from the interaction between water and varied energy of muons from low to high energy (5 MeV, 50 MeV, 100 MeV, 200 MeV, and 500 MeV) using the PHITS Monte Carlo package. PHITS is one of the licensed software that can be used in particle simulation and is user-friendly, especially for users with low computational capabilities.

2. METHOD

2.1 PHITS

The entire simulation process was carried out on PHITS software installed on a 16 GB RAM Intel Core i7 Personal Computer. PHITS (Particle and Heavy Ion Transport Code System) version 3.22 is a code that can simulate particle transport using Monte Carlo algorithms developed under collaboration between JAEA, RIST, KEK, and several other institutions (Niita et al., 2006). Many particle transport studies have been conducted using this software, such as accelerator technology(Jang et al., 2022), radiotherapy (Yani et al., 2016), space radiation (Sato et al., 2008; Aghara et al., 2015), and in many other fields related to particle and heavy ion transport phenomena. The input files for the PHITS simulation consist of source, material, geometry, and tally section. The source section is used to define the identity of the source particles, such as source type, source geometry, and particle cut-off energy. Meanwhile, the material geometry and tally sections defined the material identity that the source will pass through and the type of output required at the end of the simulation, respectively.

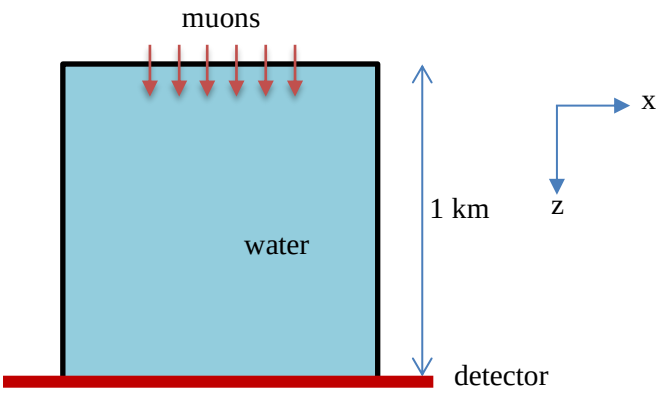

Figure 1 Simulation set-up.

2.2 Muon Source

Muons with energies of 5 MeV, 50 MeV, 100 MeV, 200 MeV, and 500 MeV are irradiated to water (H_2O) with a 1 gr/cm^3 density. This muon round source (diameter 100 cm) is placed on the water surface with dimensions of 75×75 m^2 (Figure 1). Muons are uniformly distributed on the source and are directed to move in the +z direction. The cut-off energy of all particles was set to 1×10^{-7} MeV (default value from PHITS). The number of particles simulated is 5×10^6 particles divided into five batches with the same number of particles in each batch.

2.3 Virtual Detector

Virtual detectors are placed after the water to record muon attenuation and secondary particle production during the simulation. This muon radiation technique uses muography, where the detector is simply placed after the material (1 km after the muon source is placed). This detector is dimensionless in the z-direction and is only an x-y plane with dimensions 100 × 100 m^2. The detector records all particles passing through it in the form of muons and secondary particles resulting from the interaction of muons on their journey in water. This virtual detector is set in the tally section with several input parameters, such as the virtual size of the detector, position, and type of particles to be recorded. The relative number and energy of these particles are recorded by the detector. The specific tally was set to Tally T-Product and T-track to provide the spectrum and flux particles in the detector, respectively.

3. RESULTS AND DISCUSSION

On its journey through matter, the muon will lose its energy through traces of interactions with material atoms. Like other charged particles, Muons can interact with whole atoms, orbital electrons or atomic nuclei. This affects the type of secondary particles produced, the scattering angle of secondary particles, the energy of the deposited muons, and the energy of the muons after passing through the material through multiple interactions. When a high-energy muon interacts with a nucleus, these muons are attached to the nucleus. The unstable nucleus will decay. This decay causes the atom to emit photons, Auger electrons, and neutrons through the inverse beta-decay process (Riggi, 2023). The flux of muon in the virtual detector for muon initial energy is shown in Figure 2. Although the flux map at each muon's initial energy is unchanged (the same as at the source), it is reduced due to interactions with the matter it passes through.

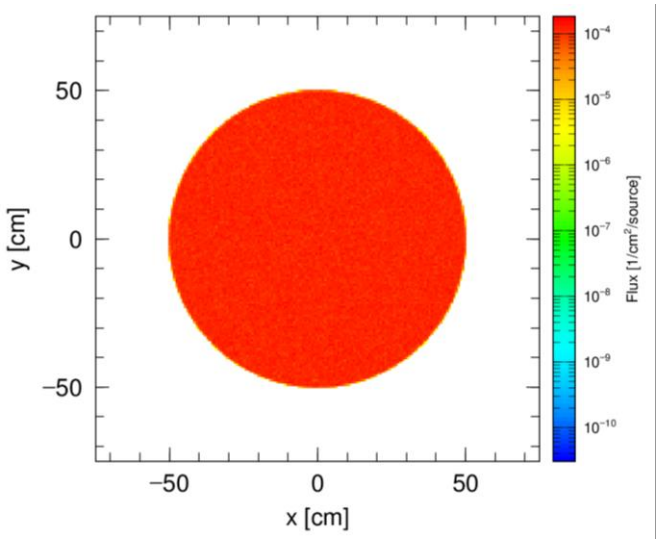

Figure 2 Muon flux recorded in the detector for muon initial energy 500 MeV.

This muon flux is the same for all muon initial energies. The muon undergoes an energy reduction on its journey that does not cause it to scatter at a large angle, and most of it remains at the

detector. These muons only experience reduced energy transferred to atoms that induce ionization, bremsstrahlung radiation, and other processes. This is because muons pass through low-density materials. The phenomenon will be different if muons pass through higher-density materials such as glass and metal. The repeated inelastic collisions of muons with atomic electrons happen when muons pass through matter. Most of these collisions lead to a minor change in the muon direction. The collective impact of these minor angle deviations accumulates, causing a final alteration in the muon's path from its initial course (Das et al., 2022). The number of collisions that occur also causes a longer simulation time where the simulation time will increase along with the increase in muon initial energy.

3.1 Flux of secondary particles

Figure 2 shows the flux of photons in the x-y plane generated by the interaction of muons and water. The flux of neutrons and photons increases as the muon energy increases. However, the scattering angle of these particles gets smaller with increasing muon energy. This result is in line with other studies that show that the magnitude of photon energy greatly affects the scattering angle (Galgóczi et al., 2020). The scattering angle is larger if the photon energy is smaller, and vice versa. High-energy photons and neutrons are concentrated in the centre of the virtual detector. These secondary particles can move and lose their energy after escaping from the water container.

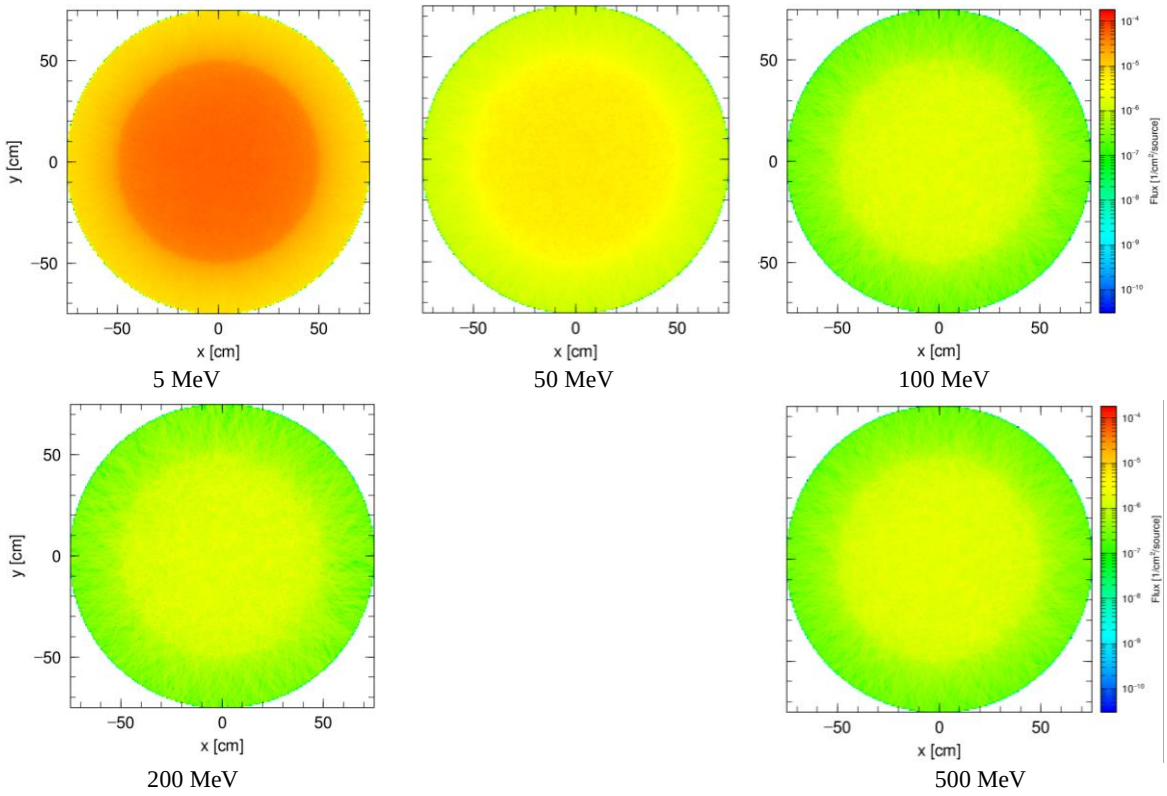

Figure 3 Photon flux recorded in the detector for muon energy of 5 MeV, 50 MeV, 100 MeV, 200 MeV, and 500 MeV.

The photon flux decreases with an increase in the muon's initial energy, as seen in the color difference map at each energy in Figure 3. At an energy of 50 MeV, the muon flux is greatest in the region with a radius of 50 m from the beam axis. Other muons are scattered to a radius of 75 m. The same pattern is also observed at higher energies but with smaller fluxes. The scattering area will be larger if a larger water phantom is used. As in photon and electron particle sources, this scattering area gets more expansive with increasing depth.

The neutron flux in detectors with different muon initial energies is shown in Figure 4. As with the photon flux, this neutron flux decreases with increasing muon initial energy. At the same energy, the

neutron flux is smaller than the photon flux. Each energy's flux is more uniform, although the beam centre shows larger values.

Muon interactions with matter can be in the form of ionization, bremsstrahlung process, pair production, nuclear interactions and hadronic capture, as obtained in this study. Photons are produced from ionization, bremsstrahlung interactions, and pair production, while neutrons are from inelastic nuclear interaction and muon and hardon capture. Other secondary particles, such as electrons and deuterons, are also possible. These secondary particles have considerable and non-negligible number and energy of particles. Low-energy photons and neutrons will undergo scattering at large angles. This result aligns with other studies conducted experimentally using a scintillator detector (Galgóczi et al., 2020; Pérez Prada et al., 2022).

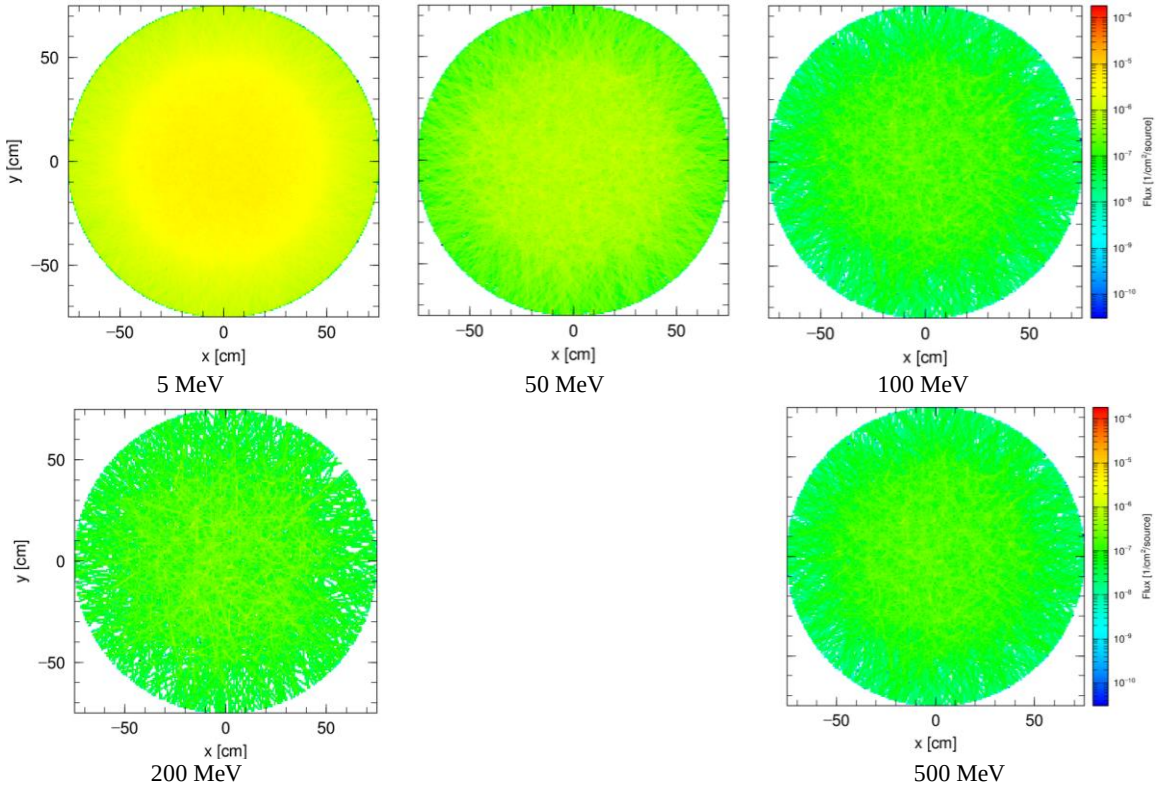

Figure 4 Neutron flux recorded in the detector for muon energy 5 MeV, 50 MeV, 100 MeV, 200 MeV, and 500 MeV.

3.2 Spectrum of secondary particles

Figure 5 below shows the spectrum of neutrons and photons produced at a 1 km distance from the muon source. The secondary particles produced are highly dependent on the muon energy of the source. The flux of neutrons and photons increases if the muon energy is minimized, especially for muons with energy less than 100 MeV. High-energy particles will move more quickly and freely than low-energy particles. Low-energy particles tend to experience interactions along their journey so that more secondary particles are produced. This phenomenon is observed not only in muon particles but also in other particles, such as photons. Neutron and electron contamination were produced during radiotherapy using photons as the sources (Yani et al., 2016).

Secondary particles and photons with an energy of 5.3 MeV are most abundant at all simulated energies. This number of photons is 10-fold greater at 5 MeV muons than at 50 MeV energy. The enormous energy of the photon was focused on the central beam axis, as confirmed in Figure 3. Meanwhile, neutrons with an energy of 3.76 are most abundant in the detector, with ten times more at an energy of 5 MeV than at 50 MeV. The number of these secondary particles (photons and neutrons)

decreases with increasing muon energy. Although at the 5 MeV muon initial energy, the flux of photons is greater than that of neutrons, the energy of neutrons is greater than the energy of photons produced.

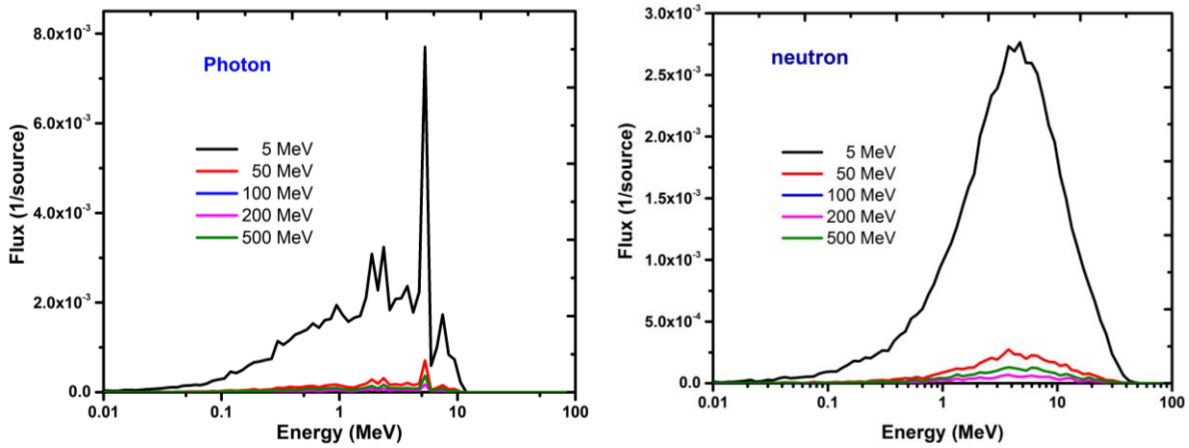

(a) (b)

Figure 5 Spectrum of (a) photon and (b) neutron produced with varied muon initial energy.

4. CONCLUSION

The simulation results show that the interaction between muons and water produces secondary particles in photons and neutrons. The energy of the source muon strongly influences the number of these secondary particles. Photons and neutrons with energies of 5.3 and 3.7 MeV, respectively, are the most abundant at all muon energies simulated. Photons result from ionization, bremsstrahlung interactions, and pair production, while neutrons originate from inelastic nuclear interactions. The secondary particle, photon and neutron spectrum show that the lower-energy muons produce more secondary particles because the lower-energy particles will experience more interactions. The energy and flux of these secondary particles cannot be ignored and require further study of their impact on living organisms.

ACKNOWLEDGEMENT

This study was fully supported by Hibah Program Penelitian Dosen Muda tahun 2023 Skema Penelitian Dasar di Lingkungan Institut Pertanian Bogor under the grant agreement number 11451/IT3/PT.01.03/P/B/ 2023.

REFERENCE

Abe, S., & Sato, T. (2017). Implementation of muon interaction models in PHITS. *Journal of Nuclear Science and Technology*, *54*(1), 101–110.

Aghara, S. K., Sriprisan, S. I., Singleterry, R. C., & Sato, T. (2015). Shielding evaluation for solar particle events using MCNPX, PHITS and OLTARIS codes. *Life Sciences in Space Research*, *4*, 79–91.

Armour, E. A. G. (2010). Muon, positron and antiproton interactions with atoms and molecules. *Journal of Physics: Conference Series*, *225*(1), 12002.

Barnoud, A., Cayol, V., Lelièvre, P. G., Portal, A., Labazuy, P., Boivin, P., & Gailler, L. (2021). Robust Bayesian joint inversion of gravimetric and muographic data for the density imaging of the Puy de Dôme Volcano (France). *Frontiers in Earth Science*, *8*, 575842.

Danev, P., Adamczak, A., Bakalov, D., Mocchiutti, E., Stoilov, M., & Vacchi, A. (2016). Low-energy negative muon interaction with matter. *Journal of Instrumentation*, *11*(03), P03019.

Das, S., Tripathy, S., Jagga, P., Bhattacharya, P., Majumdar, N., & Mukhopadhyay, S. (2022).

Muography for Inspection of Civil Structures. *Instruments*, *6*(4), 77.

Galgóczi, G., Mrdja, D., Bikit, I., Bikit, K., Slivka, J., Hansman, J., Oláh, L., Hamar, G., & Varga, D. (2020). Imaging by muons and their induced secondary particles—a novel technique. *Journal of Instrumentation*, *15*(06), C06014.

Hamar, G., Surányi, G., Varga, D., Nyitrai, G., Oláh, L., Gera, Á., Balogh, S. J., & Barnaföldi, G. G. (2022). Underground muography with portable gaseous detectors. *Journal of Physics: Conference Series*, *2374*(1), 12186.

Hansen, J. S., & Thompson, M. G. (1976). The electromagnetic interactions of cosmic ray muons in iron. *Journal of Physics G: Nuclear Physics*, *2*(7), 523.

Hu, Y., Kuang, P., Li, C., Liu, F., Wu, haibiao, Xiao, D., Zhang, P., Wang, B., Cao, X., & Wei, L. (2023). Investigation of the muonic atoms distribution in materials through monic X-rays momentum simulation using Geant4. *Physica Scripta*.

Infantino, A., Blackmore, E. W., Brugger, M., Alía, R. G., Stukel, M., & Trinczek, M. (2016). FLUKA Monte Carlo assessment of the terrestrial muon flux at low energies and comparison against experimental measurements. *Nuclear Instruments and Methods in Physics Research Section A: Accelerators, Spectrometers, Detectors and Associated Equipment*, *838*, 109–116.

Jang, Y.-J., Kwon, N. H., Park, S. H., Choi, Y., Yu, H., Kim, K. B., Kim, D. W., & Choi, S. H. (2022). Activation evaluation of Siemens linear accelerator using Monte Carlo simulation. *Journal of the Korean Physical Society*, *81*(11), 1107–1114.

Kaiser, R. (2019). Muography: overview and future directions. *Philosophical Transactions of the Royal Society A*, *377*(2137), 20180049.

Kusagaya, T., & Tanaka, H. K. M. (2015). Muographic imaging with a multi-layered telescope and its application to the study of the subsurface structure of a volcano. *Proceedings of the Japan Academy, Series B*, *91*(9), 501–510.

Mahon, D., Clarkson, A., Gardner, S., Ireland, D., Jebali, R., Kaiser, R., Ryan, M., Shearer, C., & Yang, G. (2019). First-of-a-kind muography for nuclear waste characterization. *Philosophical Transactions of the Royal Society A*, *377*(2137), 20180048.

Morishima, K., Kuno, M., Nishio, A., Kitagawa, N., Manabe, Y., Moto, M., Takasaki, F., Fujii, H., Satoh, K., & Kodama, H. (2017). Discovery of a big void in Khufu's Pyramid by observation of cosmic-ray muons. *Nature*, *552*(7685), 386–390.

Morris, C. L., Bacon, J., Borozdin, K., Fabritius, J., Miyadera, H., Perry, J., & Sugita, T. (2014). Horizontal cosmic ray muon radiography for imaging nuclear threats. *Nuclear Instruments and Methods in Physics Research Section B: Beam Interactions with Materials and Atoms*, *330*, 42–46.

Niita, K., Sato, T., Iwase, H., Nose, H., Nakashima, H., & Sihver, L. (2006). PHITS—a particle and heavy ion transport code system. *Radiation Measurements*, *41*(9–10), 1080–1090.

Nishiyama, R., Taketa, A., Miyamoto, S., & Kasahara, K. (2016). Monte Carlo simulation for background study of geophysical inspection with cosmic-ray muons. *Geophysical Journal International*, *206*(2), 1039–1050.

Oláh, L., Tanaka, H. K. M., Ohminato, T., & Varga, D. (2018). High-definition and low-noise muography of the Sakurajima volcano with gaseous tracking detectors. *Scientific Reports*, *8*(1), 3207.

Pérez Prada, M., Barnes, S., & Stephan, M. (2022). Analysis of Secondary Particles as a Complement to Muon Scattering Measurements. *Instruments*, *6*(4), 66.

Riggi, F. (2023). Interaction of Muons with Matter. In *Messengers from the Cosmos: An Introduction to the Physics of Cosmic Rays in Its Historical Evolution* (pp. 241–247). Springer.

Sakaki, Y., Namito, Y., Sanami, T., Iwase, H., & Hirayama, H. (2020). Implementation of muon pair production in PHITS and verification by comparing with the muon shielding experiment at SLAC. *Nuclear Instruments and Methods in Physics Research Section A: Accelerators, Spectrometers, Detectors and Associated Equipment*, *977*, 164323.

Sato, T., Yasuda, H., Niita, K., Endo, A., & Sihver, L. (2008). Development of PARMA: PHITS-based analytical radiation model in the atmosphere. *Radiation Research*, *170*(2), 244–259.

Vanini, S., Calvini, P., Checchia, P., Rigoni Garola, A., Klinger, J., Zumerle, G., Bonomi, G., Donzella, A., & Zenoni, A. (2019). Muography of different structures using muon scattering and absorption algorithms. *Philosophical Transactions of the Royal Society A*, *377*(2137), 20180051.

Yani, S., Dirgayussa, I. G. E., Rhani, M. F., Soh, R. C. X., Haryanto, F., & Arif, I. (2016). Monte Carlo study on electron contamination and output factors of small field dosimetry in 6 MV photon beam. *Smart Science*, *4*(2), 87–94.

Zhang, Z.-X., Enqvist, T., Holma, M., & Kuusiniemi, P. (2020). Muography and its potential applications to mining and rock engineering. *Rock Mechanics and Rock Engineering*, 1–15.